Quantifying hydrodynamic model uncertainty for robust control of wave energy devices

Mahdiyeh Farajvand, Demián García-Violini, Christian Windt, Valerio Grazioso, and John V. Ringwood

Abstract—Wave energy converter (WEC) modelling attracts significant uncertainty, often due to the need to develop compact parametric models for simulation, optimisation and control design. For linear models, which form the basis of many WEC control philosophies, this uncertainty can be as a result of real system nonlinearity, particularly as a result of control action, as well as more general uncertainty in the hydrodynamic modelling process. Recent developments in WEC control include the development of robust control algorithms, which utilise a nominal linear model, but tolerate a level of uncertainty in the model parameters. This study develops a framework for identifying a nominal model plus model uncertainty bounds, which uses data from nonlinear computational fluid dynamics (CFD) simulation. Two robust control solutions are developed, one with an analytical approach, for circular uncertainty boundaries, and a further numerical approach, considering uncertainty sets of arbitrary shape. Finally, the comparative controller performance, based on the appropriate selection of a nominal model and uncertainty bound, compared to a non-robust nominal controller, is shown.

Index Terms—Computational fluid dynamics, system identification, model uncertainty, pseudospectral, robust control, energy maximisation

I. INTRODUCTION

THE development of cost-competitive and commercial wave energy converter (WEC) technology is a challenging task. Optimal energy extraction from WECs, formulated in terms of the optimal control problem, is a solution to improve the cost competitiveness of WECs. Early work on optimal control technique for WECs for energy absorption improvement can be found in [1]. The majority of control strategies for WECs are model-based, where the control efficacy is significantly affected by the accuracy of the system model. WECs operate under the influence of the dynamics of the different conversion stages and complex fluid-structure interactions, posing considerable uncertainty in device modelling. Neglecting such uncertainty will affect the control performance. Therefore, efficiently handling WEC model uncertainty is of paramount importance in the development of model-based control strategies.

Recent studies on sensitivity and robustness issues associated with WEC controllers, which consider possible unknown model parameters, modelling errors, external disturbances and non-causal forces, can be found in [2-7]. To briefly summarise, a model focusing on the impact of wave excitation force prediction errors is proposed in [2], which is crucial for the design of non-causal robust control. Robust moment-based energy maximising optimal control of WECs, considering parametric model uncertainty is studied in [3]. The study in [4] takes an uncertain power-take off (PTO) system into account for the design of robust optimal control strategy. Estimation of numerical uncertainty in computational fluid dynamics (CFD) simulation of a point absorber WEC with a passive controller are investigated in [5]. The study performed in [6] estimates the modeling uncertainty in an online manner which is used to formulate the optimal control problem for a WEC. [7] considers a WEC subject to stochastic incident waves to investigate the energy maximising controller, designed to be robust to unstructured uncertainty.

For energy maximisation control problems, under the linear hydrodynamic model assumption of WECs, uncertainty or nonlinearity in the device model can occur as the device motion is exaggerated by control action. Investigation of the resulting modelling paradox of WECs due to control force action can be found in [8]. New modelling techniques in WECs provide a large amount of high-fidelity data. A review of nonlinear approaches for mathematical modeling of WECs is presented in [9]. CFD is a fully nonlinear model of WECs, based on solving the Navier-Stokes equations for the analysis of fluid behavior [9]. Recently, CFD-based numerical wave tank (CNWT) models capture all relevant hydrodynamic nonlinearities, including large surface deformation, viscous drag or turbulence effects [10]. CNWT models have been shown to provide high-fidelity analysis of WECs and to be a powerful tool for power production assessment [11], [12]. High-fidelity models of WECs, implementing the Navier-Stocks equations, are approximate model structures. Therefore, even nonlinear high-fidelity models of WECs can contain parametric or nonparametric uncertainty [13]. For real-time model-based control strategies, real system behaviour can be obtained by means of a local linearisation technique, where the system parameters are locally accurate at each operating point [14]. However, the control design of such a parameter-varying system increases the complexity of the problem. Moreover,

Mahdiyeh Farajvand, Valerio Grazioso, and John V. Ringwood are with the Centre for Ocean Energy Research, Maynooth University, Maynooth W23 F2H6, Ireland (e-mail: Mahdiyeh.Farajvand.2021@mumail.ie, Valerio.Grazioso@mu.ie, John.Ringwood@mu.ie).

Demián García-Violini is with Departamento de Ciencia y Tecnología, Universidad Nacional de Quilmes, Roque Saenz Peña 352, Bernal B1876, Argentina (e-mail: ddgv83@gmail.com).

Christian Windt is with Leichtweiß-Institut for Hydraulic Engineering and Water Resources. Technische Universität Braunschweig, 38106 Braunschweig, Germany (e-mail: c.windt@tu-braunschweig.de).

tracking all the potential parameter changes of the system is a difficult task. To address these challenges, recent developments in WEC control problems have focussed on robust control strategies based on a linear nominal model, together with an uncertainty bound. A methodology for representing linear hydrodynamic models of WECs, based on numerical wave tank experiments and nonlinear CFD models has been developed in [15].

The work presented in this work studies an optimal robust strategy with application to WECs, but with a specific focus on the determination of modelling uncertainty. Optimal WEC control, based on spectral and pseudospectral methods, both of which are classes of direct transcription methods, is widely considered, with applications to WECs in [16] [17] [18] [19]. In most of the literature, spectral and pseudospectral problems are considered in a non-robust sense, considering only nominal mathematical models. Recently, a novel framework is proposed which considers a nominal model plus dynamical uncertainty in the computation of robust optimal control for spectral and pseudospectral methods, for wave energy applications [20]. Accuracy in calculation of the uncertainty bound can significantly impact the WEC control function and a closer, non-conservative, fitting of the uncertainty boundary is shown to improve device performance.

The focus of this paper is on the accurate selection of the linear nominal model and quantification of uncertainty bound, based on high-fidelity nonlinear CFD simulation and the design of an optimal controller which is robust to modelling uncertainty.

The remainder of this paper is organised as follows: The WEC model is described in section II, where the numerical modeling framework, as well as the nominal and uncertainty models for robust control design, is presented. Section III details the robust controller design procedure and how uncertainty regions are defined. Section IV presents the method for nominal model determination, based on a system identification methodology, while the process for uncertainty estimation is described in Section V. Section VI demonstrates an application example, using CFD simulation, for the WEC model. Uncertainty estimation, for the example under study, is examined in Section VII, while the robust controller design example of the study is provided in Section VIII. Finally, conclusions on the overall application are drawn in Section IX.

II. WEC MODEL

The fully nonlinear model of the device is implemented in a numerical wave tank using a mesh-based CFD method. CFD numerically solves the Navier-Stokes equations. Navier-Stokes solvers have the advantage of including all nonlinear effects and providing a high-fidelity model of WECs. The OpenFOAM package is an open sourse CFD library which is used as the Navier-Stokes solver. Incompressible Reynolds average Navier-Stokes (RANS) equations, can be written [8] as:

$$\nabla \cdot (\rho(t,x)U(t,x)) = 0 \qquad (1)$$

$$\frac{\partial \rho(t,x)U(t,x)}{\partial t} + \nabla \cdot \rho U(t,x)U(t,x) = -\nabla p(t,x) +$$
$$\nabla \cdot (\mu \nabla U(t,x)) + \rho f_b(t,x) + f_u(t,x), \qquad (2)$$

where equations (1) and (2) are the conservation equations for mass and momentum, respectively. In the above equations, t is the time, U(t) is the fluid velocity field, p(t) the fluid pressure, ρ the fluid density, μ the dynamic viscosity, and $f_b(t)$ the external forces, such as gravity.

The mathematical WEC model considered for the control problem of this study is based on a common theoretical background, known as Cummin's equation. Under the assumption of an inviscid fluid and irrotational and incompressible incident flow, the equation of motion for a WEC, in terms of Cummin's equation, can be expressed [21] as:

$$(M + m_\infty)\ddot{x}_p(t) + \int_0^{+\infty} h_r(\tau)\dot{x}_p(t-\tau)d\tau +$$
$$s_h x_p(t) = f_{ex}(t) + u(t), \qquad (3)$$

where $x_p(t)$, $\dot{x}_p(t) = v(t)$ and $\ddot{x}_p(t)$ are the WEC position, velocity, and acceleration, respectively. M is the mass of the oscillating body, and m_∞ the added mass at infinite frequency. $h_r(t)$ is the radiation force impulse response, arising from the fact that device motion is affected by surrounding fluid, and s_h is hydrodynamic stiffness, related to the buoyancy force. Additionally, in Eq. (3), $f_{ex}(t)$ is the wave excitation force, produced by the action of incoming waves, and $u(t)$ represents the control force applied through the PTO system.

In this paper, a pseudospectral method is utilised to discretise the problem which approximates the states and control variables, in an N-dimensional vector space, with a linear combination of the orthogonal basis functions, $\Phi = \{\phi_i\}_{i=1}^N$. The states and the control signal of the system are commonly approximated as follows:

$$x_i(t) \approx x_i^N(t) = \sum_{j=1}^N \phi_j(t)x_{ij} = \Phi(t)\hat{x}_i \qquad (4a)$$

$$u(t) \approx u^N(t) = \sum_{j=1}^N \phi_j(t)u_j = \Phi(t)\hat{u}, \qquad (4b)$$

where weight vectors are grouped as $\hat{x}_i = [x_{i1} \cdots x_{iN}]^\intercal \in \mathbb{R}^N$, and $\hat{u} = [u_1 \cdots u_N]^\intercal \in \mathbb{R}^N$. These vectors are determined by forcing the projection of the residual functions over the set of test functions $\Psi = \{\psi_j\}_{j=1}^N$ to be zero. Using the pseudospectral method, the approximation of the equation of motion becomes the linear system [20]

$$\hat{v} = G_o(\hat{u} + \hat{e}), \qquad (5)$$

where $\hat{v} = [v_1 \ v_2 \ \cdots \ v_N]^\intercal$ corresponds to the approximation of $v(t)$, which can be obtained by a linear combination of the vectors $\hat{x}_i$, defined in Eq. (4a), and $\hat{u} = [u_1 \ u_2 \ \cdots \ u_N]^\intercal$, as stated in Eq. (4b). G_o is the system *model*, represents the mapping between $\hat{u}+\hat{e}$, which is the approximation of the input $u_i(t) = u(t) + f_{ex}(t)$, and $\hat{v}$. Additionally, in Eq. (5), $\hat{e} = [e_1 \ e_2 \ \cdots \ e_N]^\intercal \in \mathbb{R}^n$,

where the set $\{e_i\}_{i=1}^N$ contains the coefficients of the excitation force approximation on the basis $\Phi(\mathbf{T})$, i.e. $f_{ex}(t) = f_{ex}(\mathbf{T}) \approx \Phi(\mathbf{T})\hat{e}$, where $\mathbf{T} = \{t_1, t_2, \dots, t_M\}$ indicates an equally spaced time discretisation set with a sampling rate t_m. Thus, when the the Fourier set of basis functions $\Phi(t)$ are considered, as in the application case of this study in Section VIII, then

$$\Phi(\mathbf{T}) = \begin{bmatrix} \cos(\omega_1 t_1) & \sin(\omega_1 t_1) & \cdots & \cos(\omega_N t_1) & \sin(\omega_N t_1) \\ \cos(\omega_1 t_2) & \sin(\omega_1 t_2) & \cdots & \cos(\omega_N t_2) & \sin(\omega_N t_2) \\ \vdots & \vdots & \vdots & \vdots & \vdots \\ \cos(\omega_1 t_M) & \sin(\omega_1 t_M) & \cdots & \cos(\omega_N t_M) & \sin(\omega_N t_M) \end{bmatrix}$$

Thus, coefficients of the excitation force, $\hat{e}$, are computed as follows:

$$\hat{e} = (\Phi(\mathbf{T})^\mathsf{T} \Phi(\mathbf{T}))^{-1} \Phi(\mathbf{T})^T F_{ex}(\mathbf{T})$$

The basis functions are chosen such that G_o satisfies

$$G_o = \bigoplus_{k=1}^{N/2} \begin{bmatrix} \mathcal{R}_k^o & \mathcal{I}_k^o \\ -\mathcal{I}_k^o & \mathcal{R}_k^o \end{bmatrix} \tag{6}$$

where

$$\mathcal{R}_k^o = \mathbb{R}e\{g_o(j\omega_k)\}, \mathcal{I}_k^o = \mathbb{I}m\{g_o(j\omega_k)\},$$

with $\mathcal{R}_k^o, \mathcal{I}_k^o \in \mathbb{R}$, and $g_o(j\omega_k)$ represents the nominal frequency response of the system at frequencies ω_k. Additionally, $G_o \in \mathbb{R}^n$ is a block diagonal matrix and the symbol $\bigoplus$ denotes the direct sum of n matrices, i.e. $\bigoplus_{i=1}^n A_i = diag\{A_1, A_2, \cdots, A_n\}$.

For application of the robust control approach, a model of the system G is defined considering a realistic situation. The real system, based on the nominal model G_o and the uncertainty set of multiplicative type, can be formulated as:

$$G = G_o(I + \Delta_m) \tag{7}$$

where $\Delta_m \in \mathbb{R}^{N \times N}$ represents the bounded multiplicative uncertainty, and I is the identity matrix.

III. ROBUST CONTROLLER DESIGN

A. Preliminaries

1) Control problem definition: The control objective for the WEC system is to maximise the total absorbed energy. For a WEC system, which is subject to an external excitation force $F_e(t)$ and is controlled via a control force $u(t)$, the total absorbed energy over the interval $[0\ T]$, is computed as:

$$J \equiv E = -\int_0^T P dt = -\int_0^T v^\mathsf{T}(t)u(t)dt \tag{8}$$

where E is the absorbed energy, P the instantaneous power, $u(t)$ the control force applied through the PTO system, and $v(t)$ the device velocity, as defined in Eq. (3). Eq. (8) defines the objective function J for this study. The optimal control problem consists of obtaining the PTO control force $u(t)$, that maximizes the objective function J, subject to the equation of motion. Due to orthogonality of the basis functions

ϕ_j, the application of pseudospectral approximations to the objective function J results in:

$$J \approx J_N = \int_0^T \hat{u}^\mathsf{T} \Phi^\mathsf{T}(t)\Phi(t)\hat{v} = -\frac{T}{2}\hat{u}^\mathsf{T}\hat{v} \tag{9}$$

It can be easily seen how the integral relationship of Eq. (8) is transformed into an algebraic equation.

2) Nominal optimal solution: By substituting Eq. (5) into the approximate absorbed energy expression in Eq. (9), the following equality is obtained:

$$J_N = -\frac{T}{2}\hat{u}^\mathsf{T}G_o(\hat{u} + \hat{e}) \tag{10}$$

Eq. (10) is a quadratic function, in which the optimisation problem is carried out over the control variable $\hat{u}$ alone. In order to guarantee the existence of a maximum value for the objective function of the WEC, the system should be passive, i.e. its transfer function should be positive real [22]. In contrast to energy maximising problems of WECs, using boundary element methods (BEM), in which passivity of the system would be satisfied by definition, WEC modeling using experimental data does not guarantee the passivity condition. In order to meet the feasibility condition for the energy maximisation problem of a WEC, using experimental data, it is necessary to render the system passive. Guaranteeing the existence of a maximum for the objective function, Eq. (10) can be restated as:

$$\hat{u}_o^\star \leftarrow \max_{\forall \hat{u}_o \in \mathbb{R}^N} J_N \tag{11}$$

For an unconstrained quadratic problem, $\hat{u}_o^\star$, which maximises Eq. (9) is:

$$\hat{u}_o^\star = -(G_o + G_o^\mathsf{T})^{-1}G_o\hat{e}$$

The expression in Eq. (11) will be used in the robust formulation. Then, the optimal value of J_N, when Eq. (11) is substituted in Eq. (9), becomes:

$$J_N^\star = \frac{T}{2}\hat{u}_o^{\star\mathsf{T}}G_o(\hat{u}_o^\star + e)$$

B. Robust Approach: Best Worst-Case Performance (WCP)

The spectral and pseudospectral methods discussed in Section II are based on a precise description of the system. To proceed with the robust approach, we consider a realistic situation, where the system is described using the nominal *and* uncertainty model. The representation of the real system in (7) can be restated using additive uncertainty as:

$$G = G_o + \Delta_a$$

where $\Delta_a \in \mathbb{R}^{N \times N}$ represents the bounded additive uncertainty. Then the relation between the multiplicative uncertainty and additive uncertainty is:

$$\Delta_a = G_o\Delta_m,$$

Δ_a takes the following form:

$$\Delta_a = \bigoplus_{k=1}^{N/2} \begin{bmatrix} \delta_k^{\mathcal{R}} & \delta_k^{\mathcal{I}} \\ -\delta_k^{\mathcal{I}} & \delta_k^{\mathcal{R}} \end{bmatrix}$$

and the objective function J_N is redefined as:

$$J_N = -\frac{T}{2}\hat{u}^{\mathsf{T}}\bigoplus_{k=1}^{N/2}\left(\begin{bmatrix} \mathcal{R}_k^o & \mathcal{I}_k^o \\ -\mathcal{I}_k^o & \mathcal{R}_k^o \end{bmatrix} + \begin{bmatrix} \delta_k^{\mathcal{R}} & \delta_k^{\mathcal{I}} \\ -\delta_k^{\mathcal{I}} & \delta_k^{\mathcal{R}} \end{bmatrix}\right)(\hat{u}+\hat{e})$$

(12)

where $(\mathcal{R}_k^o, \mathcal{I}_k^o)$ represents the location of the nominal system. For the Fourier basis,

$$g(j\omega_k) = g_o(j\omega_k) + \delta_k \Leftrightarrow \delta_k = g(j\omega_k) - g_o(j\omega_k),$$

where $\delta_k \in \mathbb{C}$ represents the uncertainty level at the frequency ω_k with $\delta_k^{\mathcal{R}} = \mathbb{R}e\{\delta_k\}$ and $\delta_k^{\mathcal{I}} = \mathbb{I}m\{\delta_k\}$.

Considering the feasibility, the real system model, G, must be positive real [20]:

$$\mathcal{R}_k = \mathcal{R}_k^o + \delta_k^{\mathcal{R}} > 0,$$

(13)

where $\mathcal{R}_k$ is the real part of the location of the real system.

Using the feasibility condition, and defining the best-WCP solution as the input that minimises the performance degradation when the system under study is affected by a bounded uncertainty set Δ_a, the robust control problem statement can be defined as:

$$\hat{u}_r^{\star} \leftarrow \max_{\hat{u}\in\mathbb{R}^N} \min_{\Delta_a\in\mathcal{U}} J_N$$

(14)

Eq. (14) represents a robust quadratic formulation, where $\mathcal{U}$ indicates the set of all possible uncertainties. Generally, Eq. (14) can be rewritten into a minimax problem [23].

C. Uncertainty regions

Uncertainty sets can have different shapes and sizes with this section providing the solution for Eq. (14) via two different types of uncertainty representation. First, an analytical approach is proposed. The difficulty of an analytical approach is that system constraints cannot be considered in the problem. Then, a suboptimal numerical procedure, which can be applied to unstructured uncertainty, is shown. Numerical methodology has the advantage of viability to address a wide range of cases; however, in this method, the numerical complexity can grow exponentially.

1) Analytical solution approach: Different boundary schemes of the uncertainty set can be selected for the analytical solution approach. In the present study, a convex and circular boundary is considered, as shown in Fig. 1(a). $(\mathcal{R}_k, \mathcal{I}_k)$ represents the location of the real system and $\mathcal{P}_k$ is the set of all possible locations of the real system, which includes all the points on and within the hull of the geometry. Circular uncertainty sets can be defined in terms of a radius $0 \leq \rho_k \leq \bar{\rho}_k$ and an angle $0 \leq \theta_k \leq 2\pi$; thus:

$$\delta_k^{\mathcal{R}} = \mathbb{R}e\{\rho_k e^{j\theta_k}\}, \ \delta_k^{\mathcal{I}} = \mathbb{I}m\{\rho_k e^{j\theta_k}\},$$

which must be repeated for each k-block in Eq. (12). Then,

$$\mathcal{R}_k = \mathcal{R}_k^o + \delta_k^{\mathcal{R}}, \ \mathcal{I}_k = \mathcal{I}_k^o + \delta_k^{\mathcal{I}},$$

where $(\delta_k^{\mathcal{R}}, \delta_k^{\mathcal{I}})$ represents the deviation from the nominal model and $(\mathcal{R}_k, \mathcal{I}_k) \in \mathcal{P}_k$. The worst case solution will be obtained on the hull of the circle ($\rho_k = \bar{\rho}_k$).

Using a circular boundary and the analytical approach, the optimal solution [20] is:

$$\hat{u}_r^{\star} = \bigoplus_{j=1}^{N/2} -\frac{1}{2}\begin{bmatrix} 1 & \mathcal{B}_k^{\star} \\ -\mathcal{B}_k^{\star} & 1 \end{bmatrix},$$

(15)

where

$$\mathcal{B}_k^{\star} = \frac{\mathcal{I}_k^o + \bar{\rho}_k\sin\theta_k^{\star}}{\mathcal{R}_k^o + \bar{\rho}_k\cos\theta_k^{\star}}$$

The location for $\theta_k^{\star}$, where J_N reaches the minimum over the space of control inputs, is given [20] as:

$$\theta_k^{\star} = \frac{c_k^3}{\sqrt{c_k^{1^2} + c_k^{2^2}}} - \arctan\frac{c_k^1}{c_k^2},$$

(16)

with

$$c_k^1 = 2\mathcal{I}_k^o\mathcal{R}_k^o, \ \ c_k^2 = \bar{\rho}_k^2 + \mathcal{I}_k^o - \mathcal{R}_k^{o2}, \ \ c_k^3 = -2\bar{\rho}_k\mathcal{I}_k^o$$
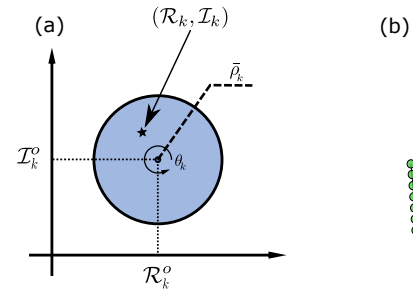

Fig. 1. (a) A convex and circular boundary of the uncertainty set. (b) Arbitrary points set.

2) Numerical solution approach: Possible uncertainty sets associated with the numerical approach include non-polytopic convex sets, polytopic convex sets, and arbitrary point sets [20]. In this study, an uncertainty set of arbitrary point type is used for the numerical approach, as shown in Fig. 1(b). The solid green points in Fig. 1(b) are those that should be included in the discretisation.

The standard minimax framework for the problem, in discrete form, is presented [20] as:

$$\min_{\hat{u}\in\mathbb{R}^N} \max_{\Delta_a^{\mathbf{i}}\in\mathcal{U}} \frac{T}{2}\hat{u}^{\mathsf{T}}G_{\mathbf{i}}(\hat{u}+\hat{e})$$

with $G_{\mathbf{i}} = G_o + \Delta_a^{\mathbf{i}}$, where $\Delta_a^{\mathbf{i}}$ is the perturbation associated at each $\mathbf{i}$-point selected for the grid.

Now, the problem can be formulated in the standard minimax form:

$$\min_{\hat{u}\in\mathbb{R}^N} \max_{\mathbf{i}} F_{\mathbf{i}}(\hat{u}) \text{ subject to } \mathcal{C}(\hat{u}),$$

(17)

where $F_{\mathbf{i}}(\hat{u}) = (T/2)(\hat{u})^{\mathsf{T}}G_{\mathbf{i}}(\hat{u}+\hat{e})$, and $\mathcal{C}(\hat{u})$ is a set of constraints. When numerical solvers are used to compute the optimal solution of the problem stated in Eq. (17), constraints can be straightforwardly included in the formulation.

IV. Nominal model determination

A. Identification test

In this study, system identification tests are performed by driving a finite-set of **N** exciting input signals, generating a corresponding set of output signals. The input signals are chosen as chirp-up signals, $f_u^i(t) = \mathcal{A}_i \sin(\omega(t)t)$, where $f_u^i(t)$ is the input force, $\mathcal{A}$ is the amplitude of the chirp signal and index i indicates the experiment number defined in accordance with each element of the set. In these tests, the device motion is excited solely by the control force $f_u^i(t)$, and no incident waves are presented; $f_{ex}(t) = \tilde{f}_{ex}(t) = 0$.

B. Model identification

This paper identifies a (nominal) linear design model via a frequency-domain black-box identification methodology. For force-to-velocity system identification, a set of chirp experiments is performed. Considering each element of the input signal set, an empirical transfer function estimate (ETFEs), $H^i(jw)$, is computed using the chirp force signal $f_u^i(t)$ and its corresponding generated output, $v_m^i(t)$ [24] as:

$$H^i(jw) = \frac{V_m^i(jw)}{F_u^i(jw)}. \tag{18}$$

C. Nominal model selection criteria

In the frequency domain, different approaches can be taken to define a nominal model, based on the ETFE. The potential approaches for selecting nominal model are:

1) *Nominal model based on experimental test*
   In this approach, a specific ETFE, which is the most representative of the system dynamics, is selected. An ETFE corresponding to a low input amplitude could result in a more representative description of the system, in terms of physical behaviour. To be more specific, a low input amplitude will generate small displacements of the WEC, satisfying the linear assumption in Cummin's equation.

2) *A synthetically-built nominal model*
   In this approach, a nominal model is built based on specific dynamical specification. In a robust control approach, a nominal model corresponding to a minimum uncertainty size will result in a less conservative controller. An important example of a nominal model corresponding to minimum uncertainty size is one based on the centre of the minimum radius circles in the complex plane, where the circles contain all the experimental responses at each frequency. In this method, the real model of the system will be included within the minimum radius circles. A similar approach, involving Gershgorin circles, also employs a set of circles of minimum radius. The Gershgorin circle theorem identifies a region in the complex plane that contains all the eigenvalues of a complex square matrix [25].

V. Uncertainty estimation

The uncertainty inherent in the WEC model is estimated by pursuing the following subsequent steps:

1) *Experiment design*: The first step in uncertainty estimation is the experiment design, where the type of input force signal, signal time length, number and amplitudes of the experimental set are chosen, based on the WEC under study.

2) *CFD simulation*: After the experiment design step, and specification of experimental set-up parameters, CFD simulations are performed, using the chosen set of exciting input signals, and corresponding output signals are obtained.

3) *ETFE computation*: This step includes the computation of ETFEs, based on the data obtained from CFD simulations.

4) *Nominal model selection*: The ETFEs of the experimental set are used to choose a sensible nominal model for the optimal control problem.

5) *Uncertainty set determination*: An appropriate uncertainty set type is chosen among the possible types of uncertainty set boundaries, as discussed in Section III-C

6) *Uncertainty estimation*: The nominal model and uncertainty set are used to quantify the model uncertainty for the robust optimal control problem.

VI. Application Example

A. Example WEC system

The wave energy device under investigation is a point absorber-type device with axisymmetric cylindrical geometry and a hemispherical bottom [8]. The schematic of the considered WEC and the dimensions of the numerical wave tank are shown in Figs. 2(a) and 2(b), respectively. The radii of the hemisphere and the cylinder of the buoy are 0.25m. Also, the height of the cylindrical section is 0.25m. The mass of the buoy is 43.67 kg, and the centre of the mass is located at a vertical distance of 0.191m from the bottom-most point of the hemisphere. The WEC structure is tested in a numerical wave tank with 3m water depth.
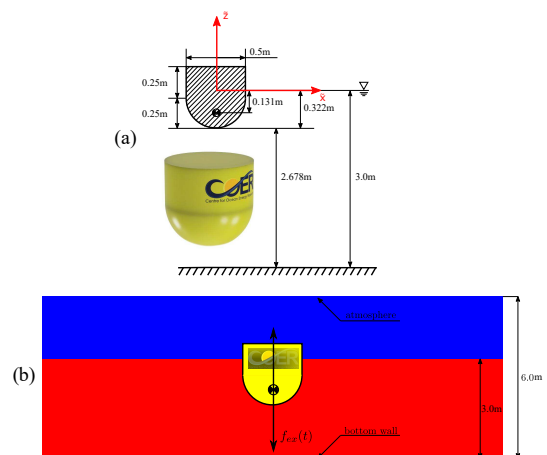

Fig. 2. Schematic of the (a) WEC structure including all relevant physical properties and (b) numerical wave tank (side view).

B. OpenFOAM model simulation

Fully nonlinear hydrodynamic simulation of the device is implemented using the open-source CFD toolbox OpenFOAM [26], where the amplitudes of the chirp-up force signals are contained in the set $\mathcal{A} = \{10, 20, 40, 50, 60\}N$ and the frequencies rate variation (chirp rate) of the chirp signals is $6Hz/s$. Each element of the set is driven by a finite-set of $\mathbf{N}$ exciting force signals (inputs), that generate a corresponding set of velocity signals (outputs). Time traces and spectral density distributions of the input and output signal of a chirp experiment, corresponding to maximum input amplitude of $\mathcal{A} = 10N$, is shown in Fig. 3.
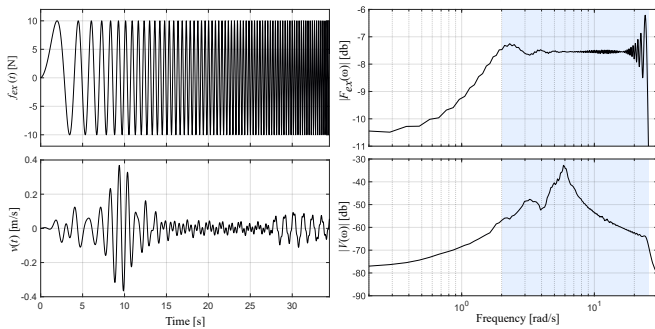
Fig. 3. Time and frequency analysis of the input chirp and output signals corresponding to maximum input amplitude of $\mathcal{A} = 10N$.

For this study, the simulation time of the chirp experiments is specified on the interval $[0\ 25]$ s. The reason for neglecting the simulation time for $t > 25$ s is the appearance of reflections in the numerical tank, which can be observed from the rise in the amplitude of the time trace velocity signals beyond 25 s in Fig. 3. The frequency range considered for this study is highlighted in the right-hand side plots of the Fig. 3 which comfortably covers the resonance frequency of the device and the frequencies around it.

C. Model identification

ETFEs (magnitude and phase) and peak resonance points, corresponding to each experiment of the set $\mathcal{A}$ with $i \in \{1, 2, 3, 4, 5\}$ where the index i indicates the experiment number defined in accordance with each element of the set of amplitudes $\mathcal{A}$, are illustrated in Fig. 4. Variability in the frequency responses, for different input amplitudes, is a clear indication of nonlinear behaviour for the system under analysis. It is worth mentioning that the obtained damping, at resonance, decreases as long as the displacement, i.e. $\mathcal{A}_i$, increases.

D. Wave excitation force specification

The control part of this study is based on the assumption of full knowledge of the wave excitation force. Wave excitation force tests are simulated in the CFD environment, where the WEC is exposed to irregular incident waves, taken from JONSWAP spectrum with a significant wave height of $Hs = 0.1m$, peak period $T_p = 1.94s$, and steepness parameter $\lambda = 3.3$. This condition represents realistic, scaled, conditions at the AMETS test site in Bellmullet, Co. Mayo, off the West Coast of Ireland [27].
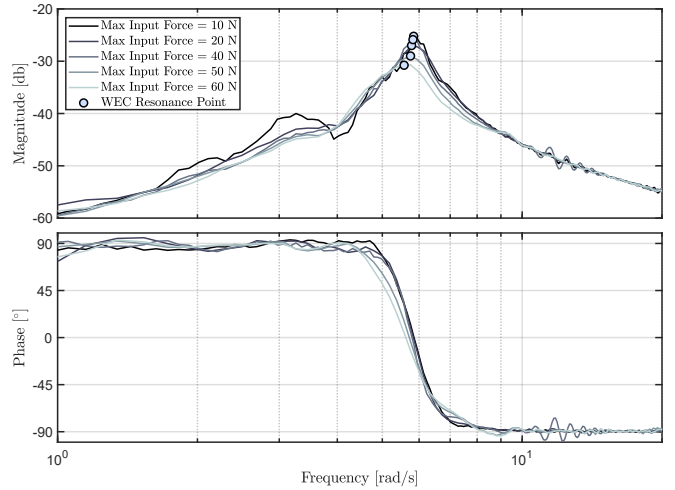

Fig. 4. Empirical transfer function estimate (ETFE) for the five experimental chirp signals
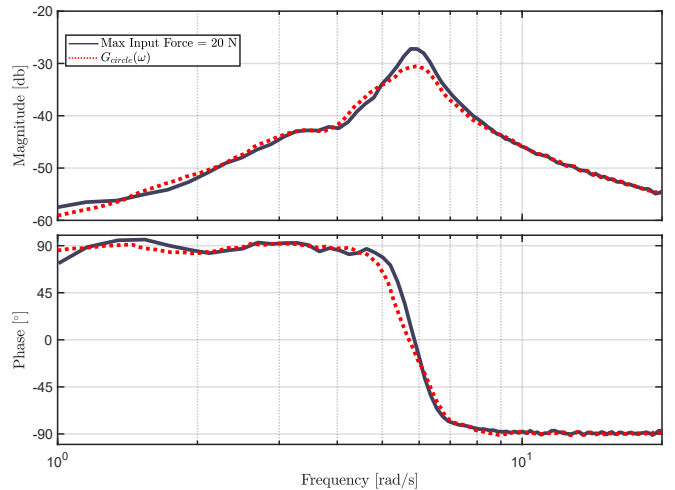

Fig. 5. Representative nominal model possibilities, based on experimentation with maximum amplitude force of 20N, and centres of the minimum radius circles.

VII. MODEL UNCERTAINTY ESTIMATION

A. Nominal model selection

In this study, two different nominal models are considered for the assessment of robust control.

A) A nominal model $G_{test}(\omega)$ based on experimentation.

In this approach, an ETFE according to the method described in IV-C(1) is considered to describe the nominal behaviour of the system. Taking the lowest amplitude of the set of input signals, $\mathcal{A}_i = 10N$, deviations related to this input signal in the ETFE are observed, as can be seen in Fig. 4. Viscous drag, limited mesh definition in the CFD environment, etc. can be a potential cause for this error. As a result, the ETFE corresponding to the amplitude of $\mathcal{A}_i = 10N$ is unlikely to be an accurate description of the system model. Consequently, the ETFE corresponding to the second lowest input amplitude, $\mathcal{A}_i = 20N$, which is the most suitable experimental representation of the system is chosen as the nominal nominal model, $G_{test}(\omega)$. $G_{test}(\omega)$ is close to the linear representation of the system where the hydrodynamic parameters are formulated under the assumption of small waves

and small body motions; thus satisfying the linear assumption in Cummins' equation.

B) A nominal model $G_{circle}(\omega)$ synthetically built to minimise the experimental uncertainty.

In this approach, the nominal model is built according to the method described in Section IV-C(2).

The two resulting nominal models considered for this study are depicted in Fig. 5.

B. Quantifying model uncertainty

In this study, in order to provide a consistent uncertainty boundary, $\Delta_m(\omega)$ must be particularly studied when:

$$\max_{1 \leqslant i \leqslant 5}\{|\Delta_m(\omega)|\} = \max_{1 \leqslant i \leqslant 5}\left\{\left|\frac{H^i(\omega) - G_o(\omega)}{G_o(\omega)}\right|\right\} \quad (19)$$

Fig. 6 shows the multiplicative uncertainty bound for the two cases of nominal models over the complete frequency range.
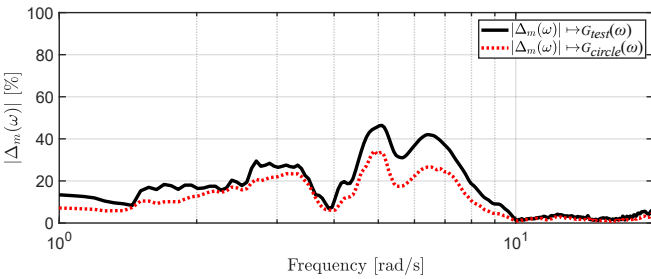
Fig. 6. Uncertainty size $|\Delta_m|$ using multiplicative uncertainty structure for two different nominal models.

Comparing the uncertainty size corresponding to the two different nominal models, $G_{test}(\omega)$ and $G_{circle}(\omega)$, it can be seen that selection of the centre of the minimum radius circles as a nominal model, results in a smaller size of multiplicative uncertainty bound, $|\Delta_m|$.

The complete model information, including ETFEs and WEC resonances, nominal models, and circular uncertainty boundaries, are presented in a Nyquist plot shown in Fig. 7, where:
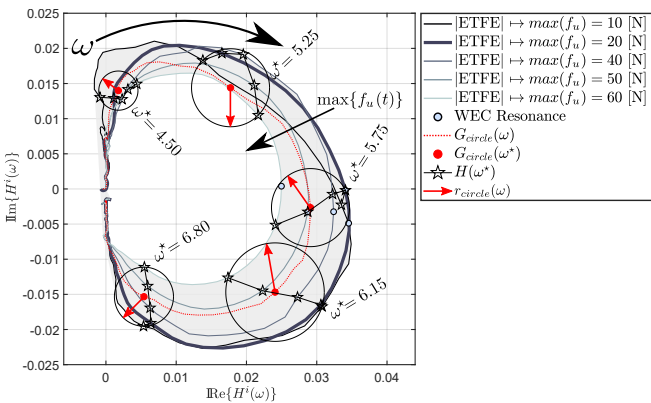

Fig. 7. Nyquist plot including ETFEs and WEC resonances, nominal models, and circular boundaries at $\omega^\star = 4.5, \omega^\star = 5.25, \omega^\star = 5.75, \omega^\star = 6.15, \omega^\star = 6.80 \ rad/s$

1) The solid lines represent the ETFEs of the set of responses related to five different maximum values of the input forces. The ETFE corresponding

to maximum force of 20N, selected as one of the nominal models in this study, is illustrated with a thick dark blue line.

2) The red dotted line represents the second nominal model scenario for this study, which is based on the centre of the minimum radius circles, containing all the experimental responses at each frequency.

3) The blue circular markers represent the location of the WEC resonance points, for each ETFE.

4) The star markers represent the ETFEs of each set for five randomly selected frequencies of $\omega^\star = 4.5, \omega^\star = 5.25, \omega^\star = 5.75, \omega^\star = 6.15, \omega^\star = 6.80 \ rad/s$, which indicate the clockwise direction for increasing ω.

5) The red circular markers represent the centre of the minimum radius circles at the five selected frequencies. Also, the radius (r_{circle}) and location of the minimum radius circles, including all the experimental points at the selected frequencies, are depicted in the Fig. 7.

C. Excitation force representation

The time domain and frequency domain data representing the wave excitation force, extracted from the numerical simulation data, are shown with the orange line in the top left and top right plots of the Fig. 8, respectively. The excitation force is approximated using 76 frequency components which perfectly cover the resonance frequency of the device and surrounding frequencies. Based on these frequency components, approximation of the excitation force is computed and the result in both time and frequency domain are shown with the blue dotted line in top plots of Fig. 8. Using 76 frequency components, good agreement between the approximated excitation wave force $\tilde{f}_{ex}(t)$ and experimental excitation wave force $f_{ex}(t)$ can be observed. In Fig. 8, the bottom left plot shows the error between $f_{ex}(t)$ and $\tilde{f}_{ex}(t)$, while the sin and cos coefficients of the excitation force, $\hat{e}$, are shown in the bottom right plot of the Fig. 8.

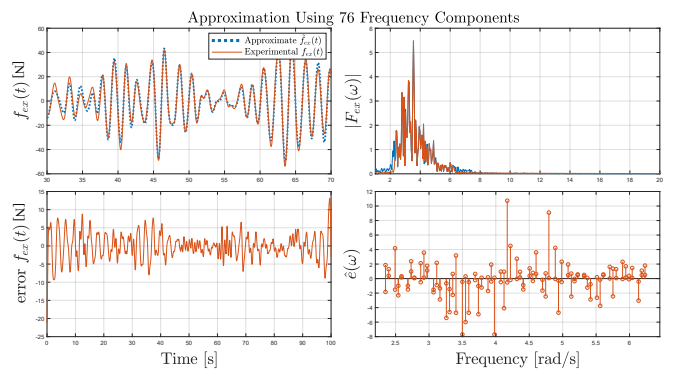Fig. 8. Experimental and approximated wave excitation force

VIII. ROBUST CONTROLLER DESIGN EXAMPLE

A. Feasibility Analysis

The real system used for the robust controller design can be discretized using 76 frequency components. The

discrete real system model in Nyquist domain, based on the second scenario nominal model, $G_{circle}(\omega)$, and a circular uncertainty bound, is represented in Fig. 9. Considering the feasibility condition for the problem described in Eq. (13), a feasible maximisation problem is satisfied only if both the nominal model and uncertainty bounds lie in the right-half complex plane. In order to meet this feasibility condition, the frequency points corresponding to the location of nominal model, and uncertainty bounds, in the left-hand plane must be omitted. Fig. 10 shows representations of the system using both nominal scenarios, $G_{circle}(\omega)$ and $G_{test}(\omega)$, where the system has been rendered to a passive type. The passive representation of the system is achieved with 22 frequency components.
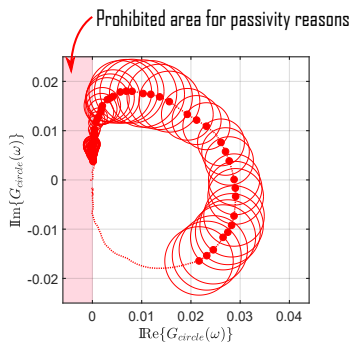

Fig. 9. Representation of the real system based on nominal model $G_{circle}(\omega)$ and circular uncertainty bound.
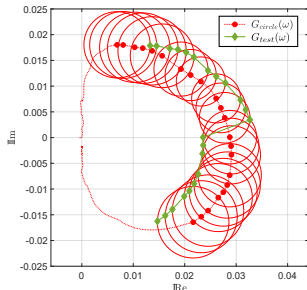

Fig. 10. Representation of a passive system approximated with 22 frequency points for the two nominal model cases.

B. Controller design

This part presents the design procedure and control performance assessment of the robust control framework introduced in Section III. Both analytical and numerical robust control designs are presented and the results are compared with an equivalent non-robust approach [16].

1) Analytical Approach: The analytical approach to the robust control problem is carried out by considering two nominal models, $G_{circle}(\omega)$ and $G_{test}(\omega)$. In this approach, two input forces for the optimal control are computed:

- $u_o(t)$, the optimal control input force is computed using the nominal approach, i.e. using the nominal model, $G_{circle}(\omega)$ and without considering any possible uncertainty.

- $u_r(t)$, the optimal control input force is computed using the robust approach, i.e. using the nominal model, $G_{circle}(\omega)$, and uncertainty bound, $r_{circle}(\omega)$.

The sin and cos frequency component coefficients for the optimal control inputs, $u_o(t)$ and $u_r(t)$ for the analytical approach are represented in Fig. 11.
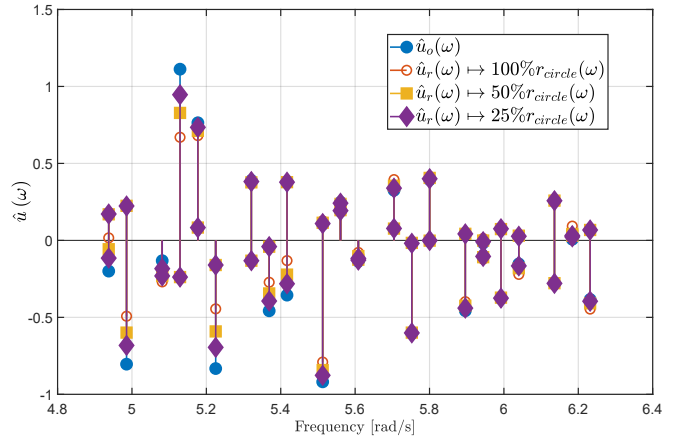

Fig. 11. Frequency components of the optimal control inputs for the analytical approach.

- The blue lines with circular markers represent the frequency component coefficients of $u_o(t)$.
- The orange lines with empty circular markers represent the frequency component coefficients of $u_r(t)$, using 100% of the radius of the uncertainty bound circles.
- The yellow lines with square markers represent the frequency component coefficients of $u_r(t)$ using 50% of the radius of the uncertainty bound circles.
- The purple lines with diamond markers represent the frequency component coefficients of $u_r(t)$ using 25% of the radius of the uncertainty bound circles.

Based on the results represented in Fig. 11, it can be concluded that by decreasing the radius of the uncertainty bound circles, the frequency component coefficients of $u_r(t)$ converge on the frequency component coefficients of $u_o(t)$. Thus, the frequency component coefficients of $u_r(t)$ using 0% of the radius of the uncertainty bound circles are equivalent to the frequency component coefficients of $u_o(t)$.

The assessment of the control performance in the analytical approach is performed using the following procedure:

1) $u_o(t)$ is applied to $G_{circle}(\omega)$ and $G_{test}(\omega)$.
2) $u_r(t)$ is applied to $G_{circle}(\omega)$ and $G_{test}(\omega)$.

Fig. 12 shows the time trace of absorbed energy for the analytical approach when $u_o(t)$ and $u_r(t)$ are applied to $G_{circle}(\omega)$ and $G_{test}(\omega)$.

- The blue line with circular markers represents the absorbed energy when $u_o(t)$ is applied to the nominal model $G_{circle}(\omega)$. This case is the ideal performance, where the optimal control input using nominal model $G_{circle}(\omega)$ is applied to the same nominal system.
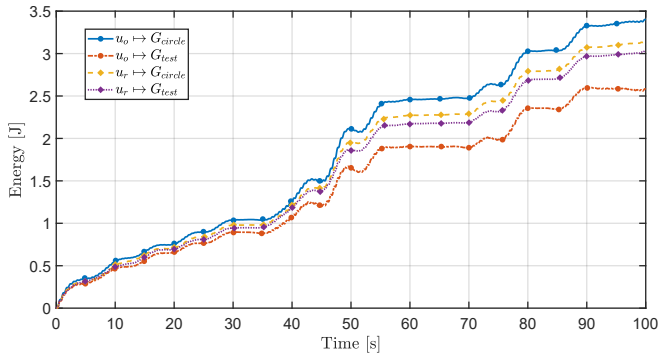
Fig. 12. Time trace of the absorbed energy for the analytical approach, applying different control input forces to the different nominal models.

Fig. 13. Frequency components of the optimal control inputs for the numerical approach.

- The orange line with circular markers represents the absorbed energy when $u_o(t)$ is applied to the nominal model $G_{test}(\omega)$. This case is the worst performance where the optimal control input using nominal model $G_{circle}(\omega)$ is applied to the nominal model $G_{test}(\omega)$.
- The yellow line with diamond markers represents the absorbed energy when $u_r(t)$ is applied to the nominal model $G_{circle}(\omega)$. In this case, the performance of the system has improved and absorbed energy of the system has moved closer to the absorbed energy for ideal performance.
- The purple line with diamond markers represents the absorbed energy when $u_r(t)$ is applied to the nominal model $G_{test}(\omega)$.

Comparing the results of applying $u_r(t)$ to the two different nominal models, the impact of the correct selection of nominal model and uncertainty bound is highlighted. In robust control, applying $u_r(t)$ to the nominal model based on the centre of the minimum radius circles ($G_{circle}(\omega)$), which corresponds to a small size of uncertainty bound, improves the control performance.

Fig. 12 shows that the mean generated power using the robust approach is always non-negative, which is in accordance with the principle of non-consumption of power using robust approaches. In this study, nominal control also results in a positive mean absorbed energy, but in the general (non-robust) case, it can take negative value [20].

2) Numerical approach: The numerical approach of the robust control is exercised using the nominal model, $G_{test}(\omega)$. In this approach, two solutions for the optimal control forces are computed:

- $u_o(t)$ is computed using the nominal approach, i.e. using the nominal model, $G_{test}(\omega)$.
- $u_r(t)$ is computed using the robust approach, based on experimental test models, $H^i(\omega)$.

The sin and cos frequency component coefficients of the optimal control inputs, $u_o(t)$ and $u_r(t)$ for the numerical approach are represented in Fig. 13. To assess the control performance of the numerical approach, the following steps are taken:

1) $u_o(t)$ is applied to $H^i(\omega)$
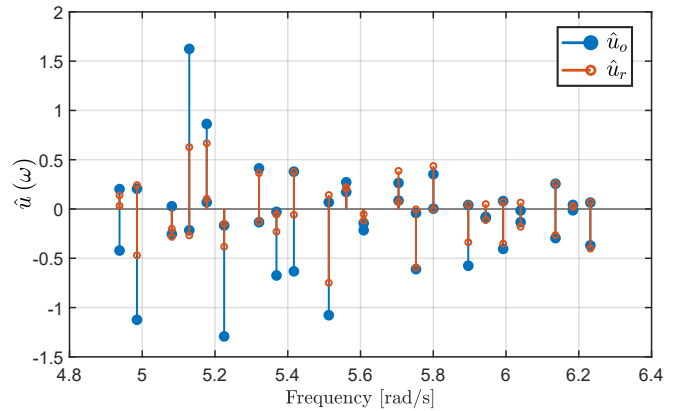2) $u_r(t)$ is applied to $H^i(\omega)$

Fig. 14 shows the time traces of the absorbed energy for the numerical approach when $u_o(t)$ and $u_r(t)$ are applied to the experimental test models and the WCP is computed at each instantaneous time.

- The blue line represents the absorbed energy when u_o is applied to the complete set of experimental models and the WCP at each instantaneous time is computed.
- The orange line represents the absorbed energy when u_r is applied to the complete set of experimental models and the WCP at each instantaneous time is computed.

Comparing the results of the absorbed energy for the two cases in Fig. 14, the advantage of using the robust approach, i.e. applying $u_r(t)$ to the real models, compared to a non-robust approach, i.e. applying $u_o(t)$ to the real models, can be seen. Using the robust control approach always results in a positive mean absorbed energy for the WEC system. Even though, applying the nominal controller to the WEC system under study resulted in a positive mean absorbed energy, it can take negative value in a general (non-robust) case.
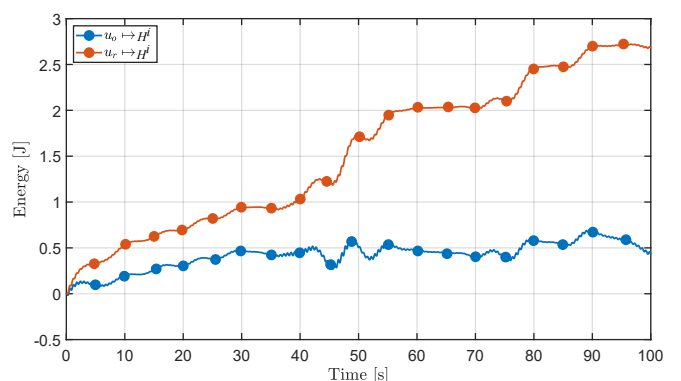

Fig. 14. Time trace of the absorbed energy for the numerical approach, applying different control input forces to the experimental test models.

IX. CONCLUSIONS

This paper focuses on WEC control design which is robust against inaccuracies, including modeling uncertainties and nonlinearities which are dominant in the

hydrodynamic model. The following conclusions can be drawn from this study:

- Modelling errors are present in all nominal models, linear or nonlinear. Estimating the parametric uncertainty for a WEC control design is as important as estimating the nominal model.
- For control design of WECs, selecting a representative nominal model and specifying the uncertainty bound as small as possible gives the least conservative control performance, as demonstrated in Fig.12.
- Robust control design based on correct specification of the nominal model and uncertainty region guarantees non-negative mean generated power.
- Even for the case of numerical modelling of WECs using CFD simulations, the passivity of the system, as presented by simulation data, cannot be guaranteed. Simulation data, or the process that generates the ETFE, are the potential causes for generating non-passive system characteristics. For the case of real data in the presence of measurement noise, the passivity condition could be more significantly violated.
- In the robust control of WECs, which preserves physical passivity, there are some unsolved problems in relation to how the nominal model and uncertainty bound can be specified. Selection of a sensible nominal model and uncertainty quantification for a non-passive wave energy systems is an important avenue for future research.

REFERENCES

[1] H. Eidsmoen, "Optimum control of a floating wave-energy converter with restricted amplitude," *Journal of Offshore Mechanics and Arctic Engineering*, vol. 118, no. 2, pp. 96–102, 1996.

[2] F. Fusco and J. Ringwood, "A model for the sensitivity of non-causal control of wave energy converters to wave excitation force prediction errors," in *Proceedings of the 9th European Wave and Tidal Energy Conference (EWTEC)*. School of Civil Engineering and the Environment, University of Southampton, 2011.

[3] J. V. Ringwood, A. Mérigaud, N. Faedo, and F. Fusco, "An analytical and numerical sensitivity and robustness analysis of wave energy control systems," *IEEE Transactions on Control Systems Technology*, vol. 28, no. 4, pp. 1337–1348, 2019.

[4] H.-N. Nguyen and P. Tona, "Robust adaptive PI control of wave energy converters with uncertain PTO systems," in *2018 IEEE Conference on Decision and Control (CDC)*. IEEE, 2018, pp. 5518–5523.

[5] W. Wang, M. Wu, J. Palm, and C. Eskilsson, "Estimation of numerical uncertainty in computational fluid dynamics simulations of a passively controlled wave energy converter," *Proceedings of the Institution of Mechanical Engineers, Part M: Journal of Engineering for the Maritime Environment*, vol. 232, no. 1, pp. 71–84, 2018.

[6] J. Na, G. Li, B. Wang, G. Herrmann, and S. Zhan, "Robust optimal control of wave energy converters based on adaptive dynamic programming," *IEEE Transactions on Sustainable Energy*, vol. 10, no. 2, pp. 961–970, 2018.

[7] Y. Lao and J. T. Scruggs, "Robust control of wave energy converters using unstructured uncertainty," in *2020 American Control Conference (ACC)*. IEEE, 2020, pp. 4237–4244.

[8] C. Windt, N. Faedo, M. Penalba, F. Dias, and J. V. Ringwood, "Reactive control of wave energy devices–the modelling paradox," *Applied Ocean Research*, vol. 109, p. 102574, 2021.

[9] M. Penalba, G. Giorgi, and J. V. Ringwood, "Mathematical modelling of wave energy converters: A review of nonlinear approaches," *Renewable and Sustainable Energy Reviews*, vol. 78, pp. 1188–1207, 2017.

[10] C. Windt, J. Davidson, and J. V. Ringwood, "High-fidelity numerical modelling of ocean wave energy systems: A review of computational fluid dynamics-based numerical wave tanks," *Renewable and Sustainable Energy Reviews*, vol. 93, pp. 610–630, 2018.

[11] C. Windt, J. Ringwood, J. Davidson, E. Ransley, M. Jakobsen, and M. Kramer, "Validation of a CFD-based numerical wave tank of the wavestar WEC," in *International Conference on Renewable Energies Offshore*, 2018, p. 439.

[12] C. Windt, J. Davidson, E. J. Ransley, D. Greaves, M. Jakobsen, M. Kramer, and J. V. Ringwood, "Validation of a CFD-based numerical wave tank model for the power production assessment of the wavestar ocean wave energy converter," *Renewable Energy*, vol. 146, pp. 2499–2516, 2020.

[13] C. Windt, N. Faedo, D. García-Violini, Y. Peña-Sanchez, J. Davidson, F. Ferri, and J. V. Ringwood, "Validation of a CFD-based numerical wave tank model of the 1/20th scale wavestar wave energy converter," *Fluids*, vol. 5, no. 3, p. 112, 2020.

[14] R. Rannacher, "Finite element methods for the incompressible Navier-Stokes equations," in *Fundamental directions in mathematical fluid mechanics*. Springer, 2000, pp. 191–293.

[15] J. Davidson, S. Giorgi, and J. V. Ringwood, "Linear parametric hydrodynamic models for ocean wave energy converters identified from numerical wave tank experiments," *Ocean Engineering*, vol. 103, pp. 31–39, 2015.

[16] G. Bacelli and J. V. Ringwood, "Numerical optimal control of wave energy converters," *IEEE Transactions on Sustainable Energy*, vol. 6, no. 2, pp. 294–302, 2014.

[17] G. Bacelli, J. V. Ringwood, and J.-C. Gilloteaux, "A control system for a self-reacting point absorber wave energy converter subject to constraints," *IFAC Proceedings Volumes*, vol. 44, no. 1, pp. 11 387–11 392, 2011.

[18] D. R. Herber and J. T. Allison, "Wave energy extraction maximization in irregular ocean waves using pseudospectral methods," in *International Design Engineering Technical Conferences and Computers and Information in Engineering Conference*, vol. 55881. American Society of Mechanical Engineers, 2013, p. V03AT03A018.

[19] R. Genest and J. V. Ringwood, "Receding horizon pseudospectral control for energy maximization with application to wave energy devices," *IEEE Transactions on Control Systems Technology*, vol. 25, no. 1, pp. 29–38, 2016.

[20] D. Garcia-Violini and J. V. Ringwood, "Energy maximising robust control for spectral and pseudospectral methods with application to wave energy systems," *International Journal of Control*, pp. 1–12, 2019.

[21] W. Cummins, "The impulse response function and ship motions," David Taylor Model Basin Washington DC, Tech. Rep., 1962.

[22] H. K. Khalil, *Nonlinear control*. Pearson Higher Ed, 2014.

[23] S. Verdu and H. Poor, "On minimax robustness: A general approach and applications," *IEEE transactions on Information Theory*, vol. 30, no. 2, pp. 328–340, 1984.

[24] D. García-Violini, Y. Peña-Sanchez, N. Faedo, C. Windt, F. Ferri, and J. V. Ringwood, "Experimental implementation and validation of a broadband LTI energy-maximizing control strategy for the wavestar device," *IEEE Transactions on Control Systems Technology*, pp. 1–13, 2021.

[25] R. S. Varga, *Geršgorin and his circles*. Springer Science & Business Media, 2010, vol. 36.

[26] H. G. Weller, G. Tabor, H. Jasak, and C. Fureby, "A tensorial approach to computational continuum mechanics using object-oriented techniques," *Computers in physics*, vol. 12, no. 6, pp. 620–631, 1998.

[27] F. Sharkey, "Dynamic electrical ratings and the economics of capacity factor for wave energy converter arrays," *European Wave Tidal Energy Conf.*, 2011.